Proceedings of the ASME 2017 36th International Conference on Ocean, Offshore and Arctic Engineering
OMAE2017
June 25-30, 2017, Trondheim, Norway

OMAE2017-62645

LABORATORY EXPERIMENTS ON ULTRASONIC LOGGING THROUGH CASING FOR BARRIER INTEGRITY VALIDATION

Andreas Sørbrøden Talberg
Dept. of Electronic Systems
NTNU
Trondheim, Norway
andreas.talberg@ntnu.no

Tonni Franke Johansen
Acoustics and Comm. Technology
SINTEF Digital
Dept. of Circulation and Medical Imaging
NTNU
Trondheim, Norway
tonni.f.johansen@sintef.no

Idar Larsen
Formation Physics
SINTEF Petroleum Research
Trondheim, Norway
idar.larsen@sintef.no

ABSTRACT

Verification of annular barriers is essential for well integrity, with ultrasonic methods being central in well integrity testing for many decades. By doing ultrasonic pitch-catch measurements on a bench top laboratory setup developed to replicate an oil well casing, we were able to show that the beam width, -6dB, of the leaky Lamb wave propagating in the pipe widens only from 14 to 20.4 mm after 140mm of propagation in the pipe. This indicates that the excited Lamb wave has beam-like features, with litle spreading perpendicular to the propagation direction, hence, can be used to evaluate a limited area of the pipe. When introducing two pipes in the experimental setup, as an extension of a previously conducted simulation study by Viggen et al. [1], we could observe multiple Lamb wave packets being excited in the pipes. By adjusting the setup to replicate casing eccentricity, the effects of this could be observed in the measurements.

NOMENCLATURE

BeCaLoS	Behind Casing Logging Setup
FEM	Finite Element Method
LLW	Leaky Lamb Waves
P&A	Plug and Abandonment
P-C	Pitch-Catch
P-E	Pulse-Echo
SNR	Signal-to-Noise Ratio

INTRODUCTION

When operating an oil or gas well or when abandoning a well when it has reached the end of its lifetime, it is of crucial importance to be in absolute control over the hydrocarbon flow. If hydrocarbons were to flow uncontrolled from the reservoirs to the surroundings, this would lead to an environmental disaster and huge costs for the responsible parties [2]. By placing a cement sheath outside the casing in a borehole, such uncontrolled flow can be prevented. This is the main objective of the cement sheath, but the sheath does also have other purposes, e.g. providing mechanical support in the well [3]. The operation of placing a successful cement sheath is difficult and requires proper planning and working knowledge of the pressure mechanics involved when placing the cement slurry [4]. Figure 1 shows different problems which may occur when the cement job is not conducted properly. Flow problems of mechanical origin may lead to the cement slurry not being placed properly, leaving areas in the annulus without cement, while problems due to degradation of the cement slurry during the curing stage may lead to defects within the sheath, such as radial fractures and enhanced porosity, leading to pollution of the cement sheath [4]. As the number of ageing oil fields reaching the end of their lifetime is increasing, the number of upcoming plug and abandonment (P&A) operations is set to quickly increase [5]. The P&A operation is an operation where the well structure is sealed to prevent oil or gas from leaking out of the well in the future. Before performing such a P&A

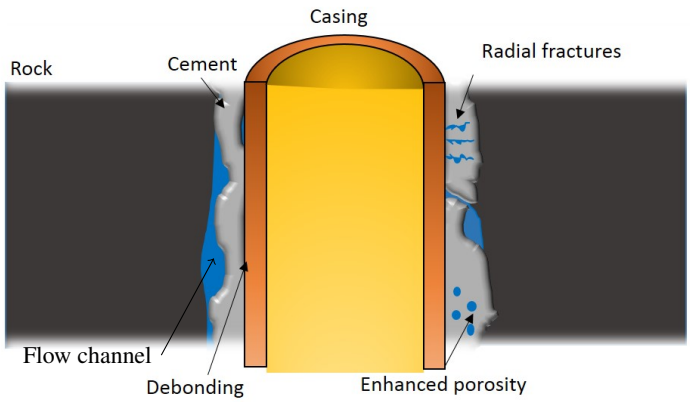

FIGURE 1: CEMENT SLURRY DISPLACEMENT PROBLEMS AND DEFECTS THAT MAY OCCUR WITHIN THE CEMENT SHEATH.

job, the quality of the cement present in the well has to be evaluated. Temperature changes, chemical processes in the well, and changes in downhole conditions that can induce stresses, can destroy the integrity of the cement sheath even though the cement sheath initially satisfied the requirements regarding isolation [6]. To ensure that a proper cement sheath has been placed, sonic and ultrasonic logging tools are widely used both to inspect the cement-to-casing bond and to detect channels where fluids can flow within the sheath [7]. Other, non-acoustic methods, are also used for cement evaluation, but the focus in this paper will be on the acoustic tools. The development of sonic tools for cement bond logging can be traced back to the 1950s and the ultrasonic tools operating at higher frequencies, typically 200 - 700kHz, were introduced in the 1960s [8]. Many of the early acoustic tools used the pulse-echo (P-E) technique to image the borehole wall. This technique, illustrated in Fig. 2, uses one transducer both as transmitter and receiver, where the transducer first emits a relative short ultrasonic pulse before it is used to detect the signal reflected at the different boundaries. As the amount of energy being reflected at each boundary are related to the acoustic impedance of the two materials at the boundary, the P-E technique can give information about the type of material outside the pipe. By analysing the received signal, information about e.g. the thickness and the internal radius of the pipe can also be found using P-E [9]. Due to the impedance of some types of light-weight cement and mud being very similar, the P-E method can come up short when trying to differentiate between these two materials in the annulus. The P-E method also have problems trying to detect defects occuring within the cement sheath [10]. The new pitch-catch (P-C) technique could potentially overcome these problems. This method involves using an ultrasonic transducer to excite elastic Lamb waves [11, 12] in the pipe. As the

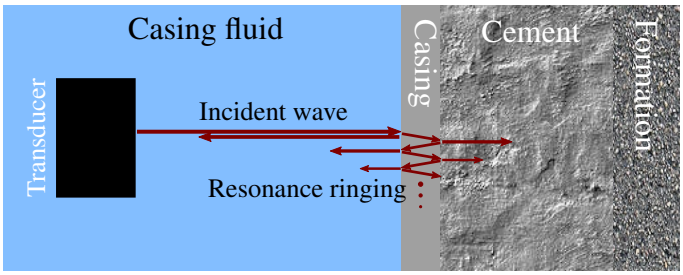

FIGURE 2: THE PULSE-ECHO TECHNIQUE.

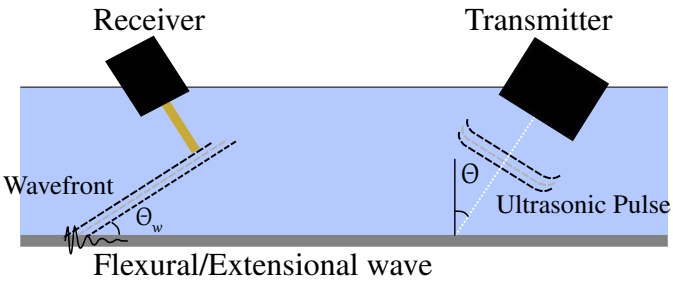

FIGURE 3: THE PITCH-CATCH METHOD.

Lamb waves propagate in the pipe, pressure waves are generated at the boundary between the pipe and the surrounding media. Hence, they are often called leaky Lamb waves (LLW). With the compressional velocity of a typical casing fluid being lower than the velocity of the elastic wave propagating in the pipe, the leaky Lamb wave acts as a supersonic sound source, radiating energy in form of a wavefront into the fluid. By using a transducer to detect this wavefront, the signal can be analysed to get information about the downhole conditions in an oil or gas well. A sketch of the pitch-catch method can be seen in Fig. 3. More profound information on Lamb waves and other elastic waves in solid media can be found in e.g. [12–17]. As described by Viggen *et al.* [1] most of the existing methods for analysing log data were developed for single-casing geometries. To use such methods to e.g. evaluate the material behind the casing in a double-casing geometry, one would have to remove the inner casings to gain access to the outer pipe. As this is a costly and time-consuming process, it would be preferable to have a method being able to log through multiple casings. A simulation study of through tubing logging were conducted in [1], and some of the results which will be presented in this paper are an experimental extension of this study.

In the following, the experimental setup will be described and the result will be presented and compared with the work done in [1]. A set of simulation results will also be presented to illustrate some of the findings in [1], and to better describe some of the experimental results. Finally, the opportunities these

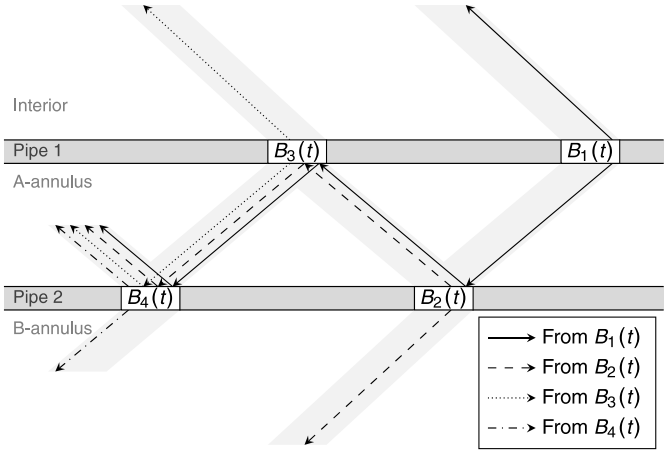

FIGURE 4: SCHEMATIC OVERVIEW OF THE INTERACTION BETWEEN LEAKY LAMB WAVE PACKETS ON TWO PARALLEL PIPES. ARROWS SHOW THE INFLUENCE FROM EARLIER WAVE PACKETS ON LATER ONES. REPRODUCED FROM VIGGEN *ET AL.* (2016) [1].

observations can bring to the field of cement evaluation will be discussed.

MATERIALS AND METHODS

Viggen *et al.* [1] describes the use of the event where multiple wave packets are excited in a system with two parallel pipes. The first wave packet in the inner pipe is excited by the transmitter in the P-C setup. As this wave packet propagates along the pipe, the wavefront radiated from it excites a wave packet in the outer pipe. This wave packet propagates in the outer pipe, radiating energy back into the annulus between the two pipes, which again excites a new wave packet in the inner pipe. After some propagation in the pipe, a train of multiple wave packets can be observed, as presented in [1] and illustrated in Fig. 4. As the first wave packet in the inner pipe, marked B_1 in Fig. 4, is excited by the transmitter in the P-C setup, it is propagating with decreasing amplitude along the pipe. Due to the observable B_3 wave packet in the inner pipe getting its energy from the two preceding wave packets (B_1 and B_2), the amplitude of B_3 will first grow, before the attenuation becomes larger than the energy it gets from the preceding wave packets, and it starts to decay. The arrows in Fig. 4 show the influence the earlier wave packets have on later ones. The time of arrival of the B_3 wave packet relative to B_1 is decided by the distance and the material in the annulus between the pipes. To detect multiple wave packets and the behaviour of their amplitudes for the case with two pipes, the pressure amplitudes have to be measured at multiple positions along the propagation direction [18].

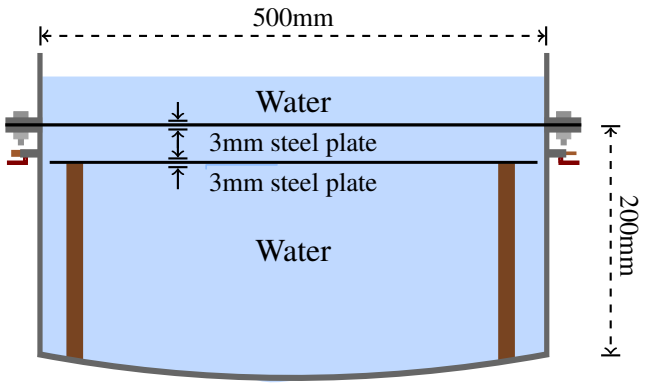

FIGURE 5: THE BECALOS WITH TWO PARALLEL PLATES AND WITH WATER IN THE ANNULUS.

The experimental work was conducted on a desktop laboratory setup at SINTEF Petroleum Research in Trondheim, Norway, called the Behind Casing Logging Setup (BeCaLoS). The setup is built as a plane layered structure with diameter 50cm. The top layer is a fluid layer, and represents the hole, where one can position ultrasonic transducers in a flexible manner. To model the well the deeper layer will typically be steel plates, representing a first casing, a solid or fluid layer, representing the first annulus, etc. The setup will be an adequate model of the well as the ultrasonic pulses used are relatively short, forms directive beams, and thus have limited spreading in the structure. The plane structure makes it relatively simple to introduce different materials in a stack. In the experiments the upper plate was a 3mm thick steel plate and the top layer was water. The experiments were conducted in two parts, on a setup with air as annulus material, and on a setup with a second plate of 3mm thickness mounted below the upper plate, surrounded by water on both sides. In the latter setup, illustrated in Fig. 5, the lower plate was mounted by placing the plate on wooden support legs. The transmitting transducer had center frequency 1MHz and its active aperture was 25.4mm (Olympus IMS C302 [19]). A center frequency of 1MHz was chosen due to the plate of the setup being 3mm thick, giving a frequency-thickness relation in the same range as in cement bond logging, making the setup a scaled model of a typical well. The acoustic field in the upper fluid layer was recorded with a hydrophone (Onda HNR-0500 [20]) with 0.5mm active aperture by moving the hydrophone in a grid of measuring points relative to the transmitter. The movement of the transducer and the hydrophone relative to each other was made relatively simple by the holder array in which the transmitter and receiver was mounted. An illustration of the holder array and the coordinate system in which the transducer was placed in origin can be seen in Fig. 6. Hence, when referring to x- and y-positions in this paper, this describes the placement of the hydrophone relative to the center of the transducer face in x- and

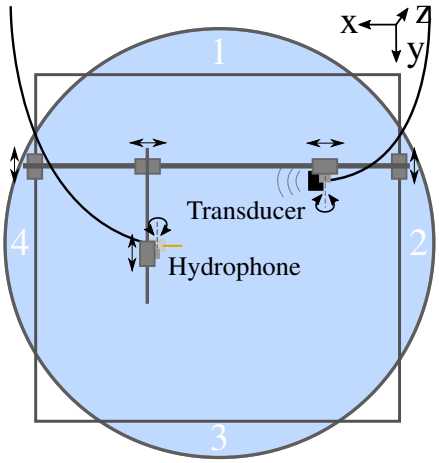

FIGURE 6: TRANSMITTING TRANSDUCER AND HYDROPHONE HOLDER ARRAY.

y-direction. The actual distance the Lamb wave propagates in the plate are shorter than these x- and y-values, as both the transducer and hydrophone are placed with a tilt in the xz-plane.

In the following, the amplitude and the behaviour of the plate wave are mentioned in several occasions. To clarify, all the measurements have been conducted by measuring the acoustic field in the upper fluid layer, and the assumption that the wave packets propagating in the plate generates the measured pressure pulses is the reason we talk about the behaviour of the plate wave.

Execution of Experimental Work

In the P-C measurements described in the following, the transducer was tilted 30° and the hydrophone was tilted 33°. Both the center of the transducer face and the hydrophone was placed 30mm above the upper plate in all the measurements. To minimize the influence of the waves being reflected at the water-air interface, surface waves were excited during the time of the measurements, and the oscilloscope, through which the detected signal was logged, was configured to take the average of 512 acquired signals. To minimize the effect of air bubbles appearing on the surfaces of the plates, which may have an effect on the coupling between the plate wave and water, the setup was tilted approximately 5°, and for each time the setup was filled with new water, it was set to rest for 24 hours before any new measurements were conducted.

To investigate the propagation of leaky Lamb waves in the plates, three sets of measurements were conducted. First with air as annulus material, moving the hydrophone in a grid with x-positions ranging from 60mm to 200mm, with 20mm intervals, and with y-positions ranging from 0mm to 80mm, with 2.5mm intervals, making a grid of 8x33 measuring points. In the measurements on the setup with two steel plates, the hydrophone was moved in a grid with x-positions ranging from 40mm to 150mm, with 10mm intervals, and with y-positions ranging from 0mm to 40mm, with 2.5mm intervals, making a grid of 12x17 measuring points, first with the two steel plates parallel to each other, then with the lower plate tilted 3.1° in the yz-plane relative to the upper plate, replicating the situation of casing eccentricity in the well. In addition to the 12x17 grid of measuring points in the setups with two plates, an additional set of measurements, moving the hydrophone from x = 40mm to x = 150mm with 2.5mm intervals, keeping y = 0mm, were conducted.

Simulation Setup

In addition to the experimental extension of the work done by Viggen *et al.* [1], 2D time domain simulations using the finite element method (FEM) solver and simulation software COMSOL Multiphysics 5.2 [21, 22] were conducted. The simulated ultrasonic pulse was excited by an inward acceleration boundary condition on the transducer face given by the equation

$$\frac{\partial^2 u_\mathrm{n}}{\partial t^2} = \boldsymbol{A} \sin\left[2\pi f_0 (t - t_\mathrm{p}/2)\right] e^{-\frac{1}{2}\left(\frac{t-t_\mathrm{p}/2}{\sigma_t}\right)^2} \sin(s\pi), \quad (1)$$

where u_n is the displacement normal to the transducer face, f_0 = 1 MHz the center frequency of the ultrasonic pulse, $t_\mathrm{p} = 4/f_0$ the pulse length, $\sigma_t = t_\mathrm{p}/8$, and s a spatial parameter running from 0 to 1 over the length of the transducer face. The amplitude $\boldsymbol{A}$ was set to $\boldsymbol{A}$ = 1 m/s^2. The geometry of the simulation setup was meshed using free triangular elements with maximum element size of $\lambda_0/6 = (c_w/f_0)/6$, where c_w is the sound velocity in the casing fluid, being 1500 m/s for water used in the simulations. To minimize the energy being reflected back into the system at the edges, the edges of the geometry were set to be low-reflecting boundaries. By logging the pressure amplitudes at 23 points placed at a height of 30 mm above the plate, at distances of 40 to 150 mm from the center of the transducer face with 5 mm intervals, the simulations could be compared with the pressure amplitudes measured by the hydrophone in the experimental work.

RESULTS

Simulations

Snapshots from the COMSOL model can be seen in Fig. 7. The figure shows the pressure, p, in the three fluid layers together with the vertical displacement, u_z, of the two plates. A pressure pulse is excited by the transducer as can be observed in the snapshot for t = 10μs. This pressure pulse excites a wave packet in the upper plate, marked (a) in the snapshot for t = 40μs in Fig. 7. As

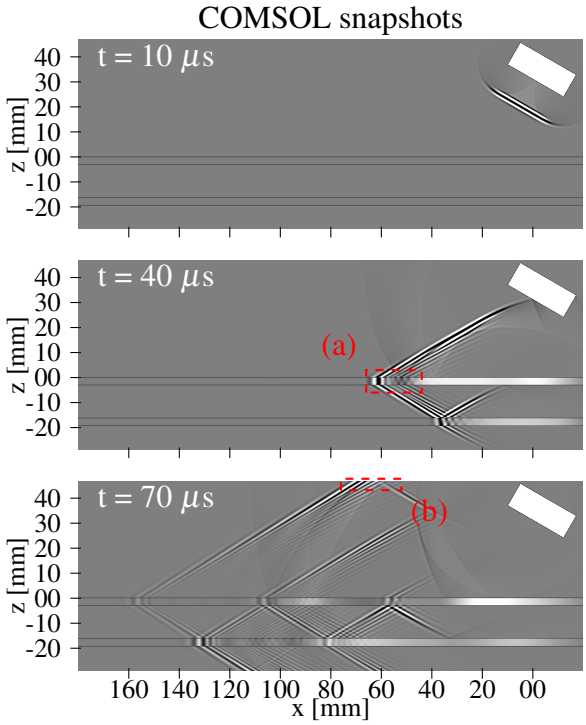

FIGURE 7: SNAPSHOTS OF PRESSURE P IN THE INTERIOR AND THE TWO ANNULUS, AND DISPLACEMENT U_Z IN PLATE 1 AND 2 AT THREE DIFFERENT TIMES.

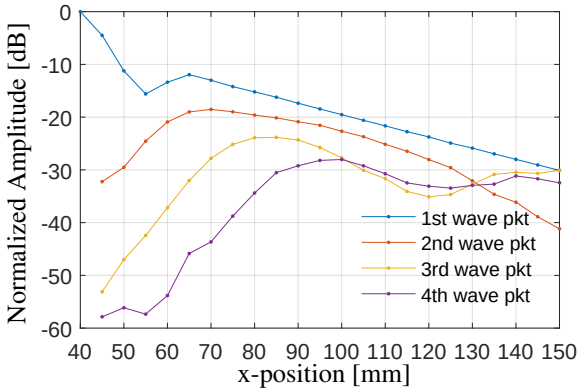

FIGURE 8: MAXIMUM AMPLITUDE OF THE VARIOUS WAVE PACKETS - COMSOL.

described by Viggen *et al.* [1], multiple wave packets, both in the upper and lower plates can be observed after some time, and the wavefronts radiated off these wave packets are clearly detectable in the pressure amplitude measurements in the simulations. By separating the different wavefronts from each other and looking at the maximum amplitude of each wavefront as a function of distance to the transducer, Fig. 8 can be plotted. From this figure it can be observed that the second, third, and fourth wave packet reaches their maxima after some propagation in x-direction, before starting to decrease. This is due to these wave packets getting their energy from the earlier wave packets, as illustrated in Fig 4.

Experimental Results

The first set of measurements were conducted on a setup with air as annulus material. The pressure, p, in the upper fluid layer which was measured by the hydrophone was stored digitally, and in the logarithmic plots presented in this paper, the pressures are plotted in decibel (dB) scale, defined as $20\log_{10}(p / p_{ref})$. In Fig 9 the amplitude measured at the eight x-positions of the hydrophone with y = 0mm are plotted logarithmically together with an linear fit. The linear fit shows a decaying amplitude in the measured pulses which decreases with α = 0.17 dB/mm along the x-axis. When the hydrophone was moved in a grid of measuring points, the amplitude of the measured pulse was found at each x- and y-position. As the amplitude decays relatively fast along the x-direction, as shown in Fig. 9, some data processing had to be conducted to more clearly show the behaviour of the plate wave amplitude as a function of distance to the transmitter (x-value). For a mesh of measurements at different x- and y-coordinates we normalize the amplitudes to the maximum value at the corresponding x-position. This gives a picture on how the plate wave behaves in the plate, and the amplitudes as a function of x- and y-position can be seen plotted logarithmic in Fig. 10. It can be observed that the elastic wave in the plate propagates as a beam, with little spreading in the direction perpendicular to the propagation direction. The beam width, where the amplitude has dropped 50% relative to the highest value, is marked by the -6dB line in Fig. 10. From 60 to 200mm from the transmitting transducer, the beam width widens only from 14 to 20.4mm, indicating a fairly collimated beam. That most of the energy is localized in a small area of the plate makes it possible to use this technique to analyse a specific area of the pipe in a downhole situation.

The second set of experimental measurements consisted of measuring on the BeCaLoS with a second 3mm thick steel plate mounted below the first. First the plates were mounted parallel to each other, with a distance of 13mm between them, second the lower plate was tilted relative to the upper plate, with a 19mm distance between the plates at y = 0mm. Fig. 11 show the results from the measurements conducted on the setup with two steel plates, both parallel and tilted. The results of the two measurements are aligned for comparison. For the set of the 45 measuring positions of the hydrophone along the x-axis, the pressure amplitudes detected were plotted logarithmic, in dB scale, as a function of x-position and time in Fig. 11a. The (a) marker in Fig. 11a highlights three of the multiple wave packets that can be

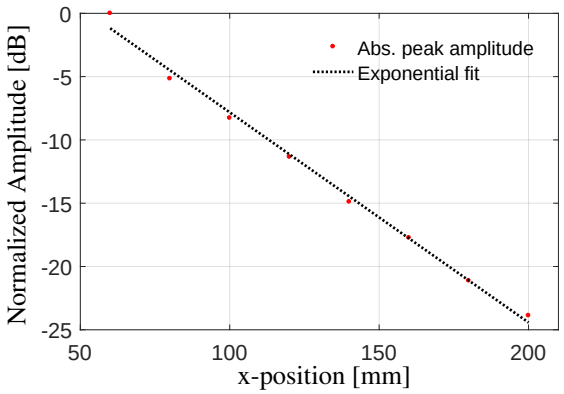

FIGURE 9: MAXIMUM AMPLITUDE OF THE WAVE PACKET - ONE PLATE - AIR IN ANNULUS.

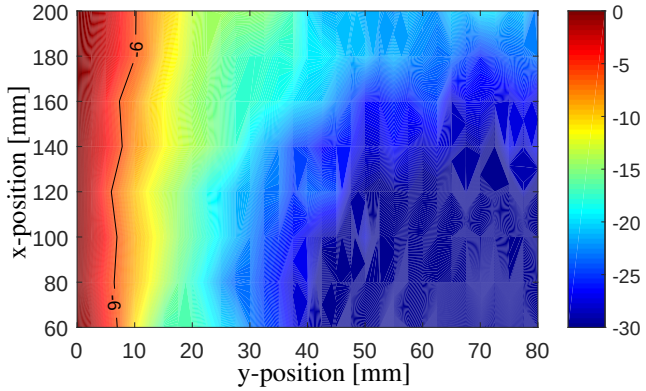

FIGURE 10: BEAM PROFILE - LOGARITHMIC (DB) PLOT OF THE WAVEFRONT AMPLITUDES - NORMALIZED AGAINST THE CORRESPONDING VALUE AT Y = 0MM - ONE PLATE - AIR IN ANNULUS.

observed in the measurements. By measuring the amplitude for each of the detectable wave packets as a function of x-position, the data plotted in Fig. 11c were found. Here, as in the figure from the simulations (Fig. 8), the characteristic behaviour of the wave packets following the first can be observed. While the energy radiated off the first wave packet is steadily decreasing, the following wave packets first grow in amplitude before starting to decay. Measuring the attenuation of the first wave packet, an attenuation value of α = 0.19 dB/mm was found by doing a linear fit on the measured data in Fig. 11c for hydrophone positions larger than x = 65mm. By moving the hydrophone in a grid of measuring points, logging the pressure for each position and normalizing the data as were done in Fig. 10, Figure 11e can be created for the first wave packet. In this figure, indicated by the -6dB line, it can be seen that the first wave packet behaves in the same manner as for the setup with air in the annulus, with most energy propagating straight forward with little spreading in y-direction. For the case with water on both sides of the plate, the detected wave front is weaker in amplitude and the attenuation is higher than for the case with air in the annulus. This is due to more energy leaking from the upper plate to the annulus between the plates. With lower amplitudes, the interference from the water propagating waves will have a more significant influence, as the signal-to-noise ratio (SNR) is lower. Marked (a) in Fig. 11e is the points where the time of arrival of the pressure wave propagating directly from the transducer to the hydrophone coincides with the time of arrival of the first wavefront. These direct waves and the distance at where they disturb the wavefront from the first wave packet can be seen marked (b) and (c) in Fig. 11a.

The final set of results is from the measurements where the lower plate was tilted relative to the upper plate. As for the two parallel plates, the absolute amplitude of the detected pulse is plotted logarithmic as a function of the x-position of the hydrophone and time in Fig. 11b, where all the signals were logged with zero displacement in y-direction. From Fig. 11b, marked (a), multiple wave fronts can be observed in the measured data. Measuring the amplitude of the first three wavefronts for each x-position along the x-axis, and plotting the amplitudes logarithmically, gives us Fig. 11d. The expected behaviour of the second and third wave packet is clearly observable, with the measured amplitudes first increasing before they start to decrease. Measuring the attenuation of the first wave packet, an attenuation value of α = 0.20 dB/mm was found by doing a linear fit on the measured data in Fig. 11d, for hydrophone positions larger than x = 65mm. When analysing the behaviour of the second and third wave packet propagating in the plate, an effect due to the tilting of the lower plate can be observed. In Fig. 11f, where the amplitude of the third wave packet is plotted logarithmic as a function of x- and y-position and normalized so the highest amplitude on each x-position is set to 0 dB, it can be seen that most of the energy now lies off the x-axis, in positive y-direction. The -6dB line in Fig. 11f, where the amplitude of the pulse is 50% relative to the highest measured amplitude, indicates that the energy in the third wave packet propagates with an angle in the xy-plane due to the tilting of the lower plate.

DISCUSSION

The experimental work conducted on a setup with air as annulus material confirmed the assumption that the plate wave propagates similar to a beam, with little spreading perpendicular to the propagation direction. This behaviour can also be observed when investigating the first wave packet in the setup with two plates. With most of the energy being localized in a narrow area along the propagation direction, this can be used to focus the inspection to a certain area of the pipe. By comparing the measured data along the x-axis for the setups with two plates, the excita-

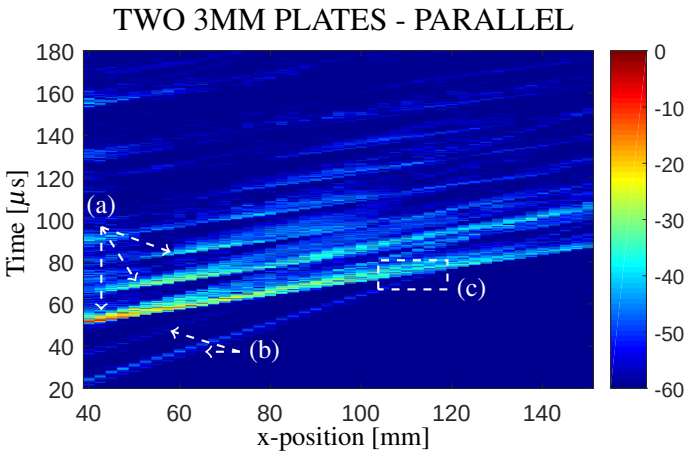

(a) AMPLITUDE OF THE DETECTED PULSE ALONG THE *X*-AXIS PLOTTED LOGARITHMIC (DB).

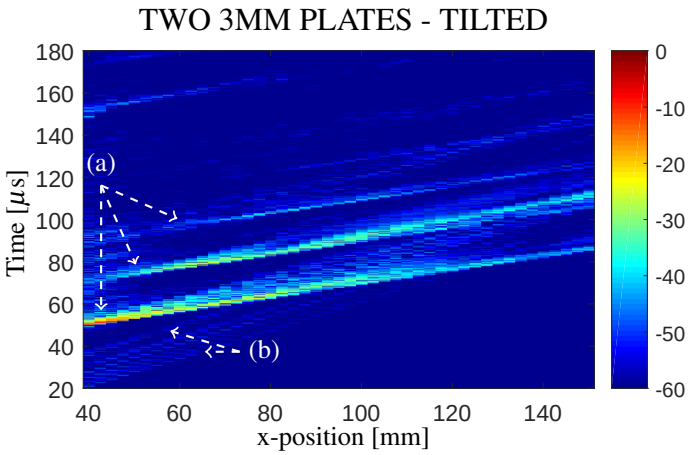

(b) AMPLITUDE OF THE DETECTED PULSE ALONG THE *X*-AXIS PLOTTED LOGARITHMIC (DB).

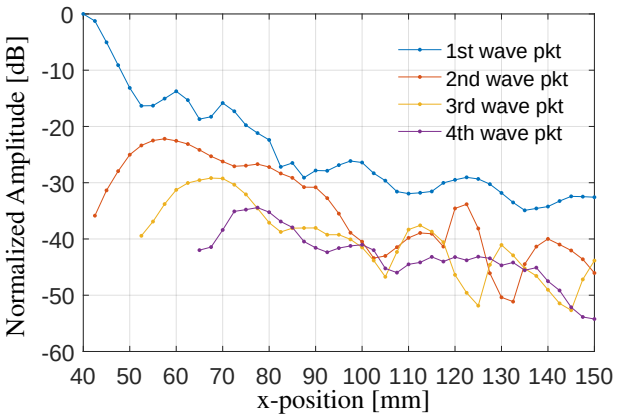

(c) MAXIMUM AMPLITUDE OF THE VARIOUS WAVE PACKETS.

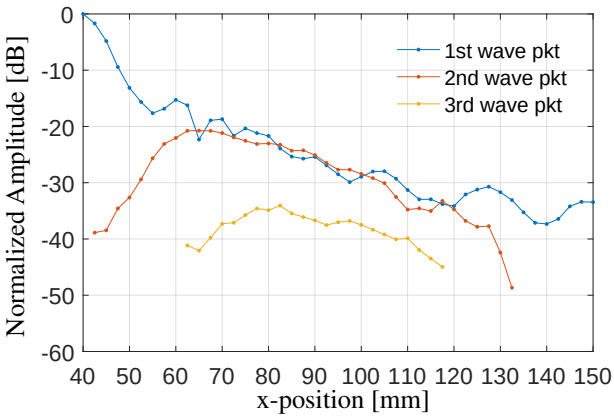

(d) MAXIMUM AMPLITUDE OF THE VARIOUS WAVE PACKETS.

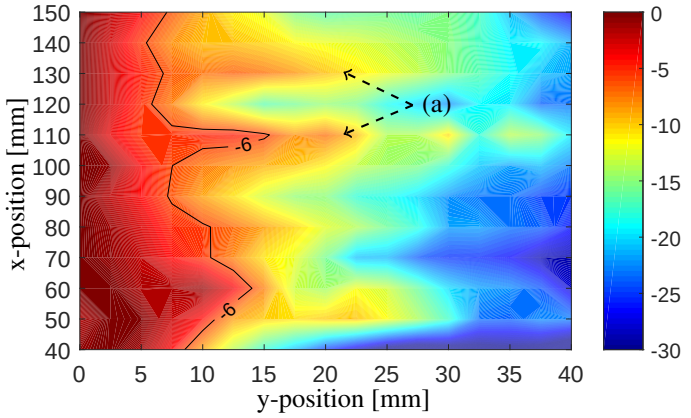

(e) BEAM PROFILE - LOGARITHMIC (DB) PLOT OF THE AMPLITUDES OF THE 1st WAVE PACKET - NORMALIZED AT EACH *X*-POSITION.

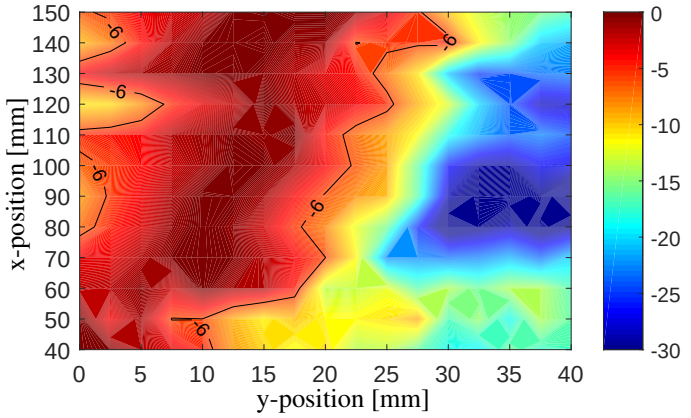

(f) BEAM PROFILE - LOGARITHMIC (DB) PLOT OF THE AMPLITUDES OF THE 3rd WAVE PACKET - NORMALIZED AT EACH *X*-POSITION

FIGURE 11

tion of multiple wave packets in the upper plate, as described by Viggen *et al.* [1], was experimentally verified. The attenuation of the first wave packet is known, and by comparing the experimental values of α = 0.19 dB/mm and α = 0.20 dB/mm with the work done by Wilcox *et al.* [16], an attenuation value of 0.2 dB/mm for the lowest order anti-symmetrical Lamb wave mode in a steel plate in water would be expected. From the COMSOL model, an attenuation value of α = 0.21 dB/mm can be found for the first wave packet. The deviation between the measured values and the values found from simulation may originate from the model being a 2D model, not taking 3D effects into consideration. The energy leaking in the directions perpendicular to the propagation direction in the measurements should lead to higher attenuation values, hence this can not explain the deviation in the attenuation values. With most of the energy propagating along the propagation direction, the 2D model is assumed to give valuable information about the physics of the measurements.

Even though the excitation of multiple wave packets was observed in the experiments, is it non trivial to confirm the theory described by Viggen *et al.* in regards to the exact growth and decay of the following wave packets. The behaviour of the following wave packets are influenced by the interaction between the pipes, which makes it hard to detect the material outside the outer pipe. In the bench top setup, bubbles on the surfaces of the plates was assumed to play a role in the measurements, altering the coupling between the plate wave and the surrounding water. By analysing the time of arrival of the different wave packets, having knowledge about the fluid between the pipes, the distance between the pipes can be found. Being able to measure by moving the hydrophone in a grid makes it possible to detect tilting of the plates relative to each other. This is done by observing that more of the energy of the plate wave lies off the x-axis. By doing further work on the setup with tilted plates, it would be of interest to make an inversion model that could be able to detect casing eccentricity in a well.

As the pressure is measured in the water layer on top of the upper plate, the measurements suffer from some interference from water propagating waves as the time of arrival of these waves coincide with the different wave packets. By increasing the distance between the transmitter and the receiver this problem can be avoided, but then an issue with the SNR due to the plate wave attenuation arise.

CONCLUSIONS

In this work we first showed through experimental measurements that the Lamb wave excited in a plate or pipe propagates in the same manner as a beam, with most of its energy limited to a narrow area along the propagation direction. For the case with air in the annulus, the beamwidth, where the amplitude has been reduced by 50% relative to the center of the beam, only widens from 14mm to 20.4mm after propagating 140mm in the plate. This property of the Lamb wave can be used to inspect a limited area of a pipe when using the P-C method for well inspection.

In the setup with two plates we observe that a series of wave packets are excited, where the amplitude of the 2nd, 3rd, etc. wave packet first increase before starting to decrease. This coincides with the simulations and the model which where presented in Viggen *et al.* [1].

The effect of tilting the plate in the casing, replicating casing eccentering in the well, is observed with 2D measurements. In these experiments the 3rd wave packet keeps its beam-like features, but tilted due to the lower plate. This could possibly be used to establish a simplified model of the wave propagation in a multiple casing situation based on ray tracing. Casing eccentering can also be measured with other methods, e.g. by using the time of arrival of the different wave packets in a P-C setup.

ACKNOWLEDGMENT

The Center for Innovative Ultrasound Solutions, CIUS, has been providing funding to this work. The bench top laboratory setup, the Behind Casing Logging Setup, was developed through funding from Statoil.

REFERENCES

[1] Viggen, E. M., Johansen, T. F., and Merciu, I.-A., 2016. "Simulation and modeling of ultrasonic pitch-catch through-tubing logging". *Geophysics,* ***81***(4), pp. D383–D393.

[2] Frigaard, I., Pelipenko, S., et al., 2003. "Effective and ineffective strategies for mud removal and cement slurry design". In SPE Latin American and Caribbean Petroleum Engineering Conference, Society of Petroleum Engineers.

[3] Calvert, D., 2005. *Well cementing*. Schlumberger, ch. preface.

[4] Allouche, M., Guillot, D., Hayman, A. J., Butsch, R. J., and Morris, C. W., 2005. *Well cementing*. Schlumberger, ch. 5.

[5] Liversidge, D., Taoutaou, S., Agarwal, S., et al., 2006. "Permanent plug and abandonment solution for the north sea". In SPE Asia Pacific Oil & Gas Conference and Exhibition, Society of Petroleum Engineers.

[6] Roy-Delage, L., Baumgarte, C., Thiercelin, M., Vidick, B., et al., 2000. "New cement systems for durable zonal isolation". In IADC/SPE Drilling Conference, Society of Petroleum Engineers.

[7] Bellabarba, M., Bulte-Loyer, H., Froelich, B., Le Roy-Delage, S., van Kuijk, R., Zeroug, S., Guillot, D., Moroni, N., Pastor, S., and Zanchi, A., 2008. "Ensuring zonal isolation beyond the life of the well". *Oilfield Review,* ***20***(1), pp. 18–31.

[8] Allouche, M., Guillot, D., Hayman, A. J., Butsch, R. J., and Morris, C. W., 2005. *Well cementing*. Schlumberger, ch. 15.

[9] Hayden, R., Russell, C., Vereide, A., Babasick, P., Shaposhnikov, P., May, D., et al., 2011. "Case studies in evaluation of cement with wireline logs in a deep water environment". In SPWLA 52nd Annual Logging Symposium, Society of Petrophysicists and Well-Log Analysts.

[10] van Kuijk, R., Zeroug, S., Froelich, B., Allouche, M., Bose, S., Miller, D., Le Calvez, J.-L., Schoepf, V., Pagnin, A., et al., 2005. "A novel ultrasonic cased-hole imager for enhanced cement evaluation". In International Petroleum Technology Conference, International Petroleum Technology Conference.

[11] Lamb, H., 1917. "On waves in an elastic plate". *Proceedings of the Royal Society of London. Series A, Containing papers of a mathematical and physical character*, pp. 114–128.

[12] Viktorov, I. A., 1967. *Rayleigh and Lamb waves: physical theory and applications*. Plenum Press, ch. II, pp. –.

[13] Alleyne, D. N., and Cawley, P., 1992. "The interaction of lamb waves with defects". *Ultrasonics, Ferroelectrics, and Frequency Control, IEEE Transactions on,* ***39***(3), pp. 381–397.

[14] Løvstad, A., 2012. "Detection of localised corrosion in pipes using guided waves".

[15] Hovem, J. M., 2012. *Marine Acoustics: The Physics of Sound in Underwater Environments*. Peninsula publishing, ch. 15 - Elastic waves in solids.

[16] Wilcox, P., Lowe, M., and Cawley, P., 2001. "Mode and transducer selection for long range lamb wave inspection". *Journal of intelligent material systems and structures,* ***12***(8), pp. 553–565.

[17] Talberg, A. S., 2016. "Experimental evaluation of broadband wave propagation in plates". Master's thesis, Norwegian University of Science and Technology.

[18] Viggen, E. M., Johansen, T. F., and Merciu, I.-A., 2017. "Simulation and inversion of ultrasonic pitch-catch through-tubing well logging with an array of receivers". *NDT & E International,* ***85***, pp. 72–75.

[19] Olympus-IMS. Olympus Panametrics C302 - Transducer. http://www.olympus-ims.com/en/ultrasonic-transducers/immersion/. Accessed: 20.11.2015.

[20] Onda Corp. Onda HNR data sheet. Revised: October 15, 2015.

[21] COMSOL Multiphysics, 2015. *Acoustic Module–Users Guide*.

[22] COMSOL Multiphysics, 2015. *Structural mechanics – Users Guide*.